The delayed response of the troposphere-stratosphere-mesosphere coupling to the 2019 southern SSW

Chengyun Yang[1], Tao Li[1], Dexin Lai[1], Xinyue Wang[2], Xianghui Xue[3], and Xiankang Dou[1]

[1]University of Science and Technology of China
[2]National Center for Atmospheric Research
[3]School of Earth and Space Sciences, University of Science and Technology of China

January 20, 2023

Abstract

A strong Southern Hemisphere (SH) sudden stratospheric warming (SSW) event occurred in September 2019 and significantly weakened the stratospheric polar vortex. Due to the positive zonal wind anomalies in the troposphere, the barotropic/baroclinic instability, primarily controlled by the horizontal/vertical wind shear, weakened in the upper troposphere at midlatitudes in late September and early October. As a result, planetary waves (PWs) were deflected equatorward near the tropopause rather than upward into the stratosphere, resulting in less perturbation to the stratospheric polar vortex. After October 15, the westward zonal wind anomalies propagate downward and reach the troposphere, increasing the tropospheric barotropic/baroclinic instability. This benefits the propagation of PWs into the stratosphere, leading to the early breaking of the stratospheric polar vortex. In turn, the SH mesosphere becomes anomalously cold due to the stratospheric wind filtering on the gravity waves (GWs), leading to the much earlier onset of SH polar mesospheric clouds (PMCs).

The delayed response of the troposphere-stratosphere-mesosphere coupling to the 2019 southern SSW

Chengyun Yang[1,2,3], Tao Li[1,2,3*], Dexin Lai[1], Xinyue Wang[5], Xianghui Xue[1,2,3] and Xiankang Dou[1,2,3,4]

[1]CAS Key Laboratory of Geospace Environment, School of Earth and Space Sciences, University of Science and Technology of China, Hefei, Anhui, China

[2]Mengcheng National Geophysical Observatory, School of Earth and Space Sciences, University of Science and Technology of China, Hefei, China

[3]CAS Center for Excellence in Comparative Planetology, University of Science and Technology of China, Hefei, Anhui, China

[4]School of Electronic Information, Wuhan University, Wuhan, Hubei, China

[5]Advanced Study Program, National Center for Atmospheric Research, Boulder, CO, USA

Corresponding author: Tao Li (litao@ustc.edu.cn)

Abstract

A strong Southern Hemisphere (SH) sudden stratospheric warming (SSW) event occurred in September 2019 and significantly weakened the stratospheric polar vortex. Due to the positive zonal wind anomalies in the troposphere, the barotropic/baroclinic instability, primarily controlled by the horizontal/vertical wind shear, weakened in the upper troposphere at midlatitudes in late September and early October. As a result, planetary waves (PWs) were deflected equatorward near the tropopause rather than upward into the stratosphere, resulting in less perturbation to the stratospheric polar vortex. After October 15, the westward zonal wind anomalies propagate downward and reach the troposphere, increasing the tropospheric barotropic/baroclinic instability. This benefits the propagation of PWs into the stratosphere, leading to the early breaking of the stratospheric polar vortex. In turn, the SH mesosphere becomes anomalously cold due to the stratospheric wind filtering on the gravity waves (GWs), leading to the much earlier onset of SH polar mesospheric clouds (PMCs).

Plain Language Summary

A rare sudden stratospheric warming event, characterized by the dramatic increase in temperature and the weakening of the stratospheric circumpolar flow, occurred in September 2019. The anomalous wind induced by the SSW event tends to propagate downward in the following months. The induced anomalous wind shear can modulate the atmospheric barotropic/baroclinic instability, guiding the propagation of the waves.

Along with the downward propagation of the SSW-induced perturbation, the atmospheric instability increases and benefits the atmospheric waves propagating into the stratosphere from late October to November. The waves propagate into the stratosphere, interact with the mean flow, and contribute to the reversal of the stratospheric zonal wind. The break of the stratospheric polar vortex can also affect the mesosphere by filtering the small-scale gravity waves, resulting in the perturbation of the temperature, water vapor distribution and the formation of clouds in the mesosphere.

Key Points

1 A rare Southern Hemisphere SSW event occurred in September 2019 and contributed to the early onset of PMCs in November.

2 The downward propagation of the zonal wind anomaly affects the propagation of PWs by modulating barotropic/baroclinic instability.

3 The secondary enhanced upward propagation of the PWs causes a delayed response in both the polar stratosphere and mesosphere.

1 Introduction

Sudden stratospheric warming (SSW), one of the most dramatic stratospheric events, is identified as minor warming when the stratospheric meridional temperature gradient reverses or major warming when the stratospheric circumpolar westerly jet completely reverses (Andrews et al., 1987; Butler et al., 2015). While major SSWs occurred approximately six times per decade in the Northern Hemisphere (NH), there was only one major SSW in 2002, and one minor but intense SSW in 2019 was recorded thus far in the SH (Baldwin et al., 2003) due to relatively weak planetary wave activity in the Southern Hemisphere (SH). Although classified as minor, according to the standard World Meteorological Organization (WMO) definition (Butler et al., 2015), the SSW that occurred in September 2019 in the SH was associated with the strongest polar-cap warming and the second strongest circumpolar westerly jet deceleration from 1979 to the present (Yamazaki et al., 2020; Shen et al., 2020a and 2020b).

SSWs in the SH have been shown to significantly impact both the troposphere and stratosphere despite their rarity (Thompson & Solomon, 2002; Thompson et al., 2005). Via the downward control principle and wave-flow interaction, the influence of SSW in the polar troposphere and stratosphere can persist for months (Baldwin & Dunkerton, 2001; Plumb and Semeniuk, 2003; Jucker & Goyal, 2022). In particular, stratospheric polar vortex variations and their downward coupling to the troposphere are regarded as critical drivers of the SH surface temperature, southern annular mode

(SAM), and southern stratospheric polar vortex (SSPV) in austral spring and summer (Thompson and Wallace, 2000; Thompson et al., 2005).

Previous studies have focused on the role of SSPV in driving climate variability at the Antarctic surface (Thompson and Wallace, 2000, Kwok and Comiso, 2002, Thompson and Solomon, 2002, Thomson et al., 2005). The variation in the lower atmosphere could potentially affect the propagation and excitation of planetary waves (PWs), which play an essential role in modulating vertical coupling from the stratosphere to the mesosphere (Garcia-Herrera et al., 2006; Black & McDaniel, 2007; Li et al., 2013; Yang et al., 2017). Stratospheric PW activity is influenced by, for example, atmospheric temperature and wind patterns, which modulate the propagation and refraction of PWs (Matsuno, 1970; Baldwin et al., 2021). The atmospheric condition for the upward PW propagation is theoretically related to the variability of the potential vorticity perturbations, which is controlled by the zonal wind and the barotropic/baroclinic instability (Charney and Drazin, 1961; Matsuno, 1970; Hartman, 1983; Meyer & Forbes, 1997). Hence, persistent atmospheric perturbation induced by SSW could potentially influence the propagation and refraction of upward PWs from the lower troposphere to the stratosphere. The convergence or divergence of planetary waves then affects the temperatures and wind patterns. This two-way feedback between the waves and wind patterns is called the wave-mean-flow interaction (Andrews et al., 1987).

Due to the filtering of gravity waves (GWs) by the stratospheric zonal wind

(Lindzen, 1981; McLandress, 1998), the variation in the stratospheric temperature gradient and the winds could effectively modulate the mesospheric circulation and thus temperature (e.g., Shepherd, 2000; Karlsson et al., 2011; Li et al., 2016). Polar mesospheric clouds (PMCs), also known as noctilucent clouds (NLCs), are the highest clouds on Earth that form in the polar summer mesopause region and are considered to be important indicators of variations in temperature and circulation in the mesosphere (Thomas et al., 1996; Hervig et al., 2009 and 2015). The earlier onset of SH PMC (Solodovnik et al., 2021) also suggested irregular variation in the SH middle atmosphere in the austral spring of 2019. The potential persistent influence of SSW on vertical middle atmospheric coupling, however, has not been well established.

The 2019 SH SSW provides an excellent opportunity to understand the coupling process of different layers of the atmosphere in the seasonal evolution process. This study explores the possible dynamic mechanism of the delayed impacts of the 2019 SH SSW on the vertical SH troposphere-stratosphere-mesosphere coupling from September through November.

2 Data and Method

The Microwave Limb Sounder (MLS) onboard the Aura satellite, launched in July 2004, measures the middle atmosphere temperature and water vapor profiles between

261 and 0.001 hPa (~92 km) from 118- and 240-GHz radiances of O2 spectra (Schwartz et al. 2008; Waters et al., 2006; Livesey et al., 2017). The latitudinal coverage of the Aura/MLS measurements is ~82°S-82°N. In this study, we calculate the daily zonal mean temperature and water vapor mixing ratio from the MLS version 4.2 dataset between August 2004 and December 2021 (available at https://disc.gsfc.nasa.gov/datasets/ML2T_005/summary).

Modern-Era Retrospective analysis for Research and Applications version 2 (MERRA-2) (Gelaro et al., 2017) temperature and water vapor (obtained from the specific humidity) data are utilized to perform diagnostic analysis and illustrate the variations in the background atmosphere. The vertical coverage of the MERRA-2 reanalysis data is from the surface to 0.01 hPa (~80 km). The Eliassen-Palm (EP) flux and its divergence were calculated according to the transformed Eulerian-mean (TEM) equations (Andrews et al., 1987; Eliassen & Palm, 1960):

$$f_{\emptyset} = \rho_0 \, a \cos\phi \, (\bar{u}_z \overline{v'\theta'}/\bar{\theta}_z - \overline{v'u'}); \quad (1)$$

$$f_p = \rho_0 \, a \cos\phi\{[f - (a\cos\phi)^{-1}(\bar{u}\cos\phi)_{\phi}] \, \overline{v'\theta'}/\theta_z - \overline{w'u'}\}; \quad (2)$$

$$Div \equiv (a\cos\phi)^{-1} \frac{\partial}{\partial\emptyset} (f_{\emptyset} \cos\emptyset) + \frac{\partial f_p}{\partial z}; \quad (3)$$

where *u, v, w,* and θ are the zonal, meridional and vertical wind, potential temperature, ρ_0, a, ϕ, f represents the air density, Earth's radius, latitude, and Coriolis parameter, respectively; the subscripts ϕ and z denote the latitudinal gradient and the vertical gradient, respectively; the overbar indicates the zonal mean value, while prime indicates the zonal anomalies.

The residual mean meridional circulation was employed to characterize the mesospheric variation response to wave activities:

$$\bar{v}^* \equiv \bar{v} - \rho^{-1}\left(\rho\,\overline{v'\theta'}/\,\bar{\theta}_z\right)_z; \tag{4}$$

$$\bar{w}^* \equiv \bar{w} + (a\cos\emptyset)^{-1}\left(\cos\emptyset\,\overline{v'\theta'}/\,\bar{\theta}_z\right)_\emptyset; \tag{5}$$

The meridional gradient of the quasi-geostrophic potential vorticity ($\bar{q}_\phi$) is used to indicate the atmospheric baroclinic/barotropic instability (Meyer & Forbes, 1997) and is expressed as:

$$\bar{q}_\emptyset = 2\,\Omega\cos\emptyset - \left(\frac{(\bar{u}\cos\emptyset)_\emptyset}{a\cos\emptyset}\right)_\emptyset - \frac{a}{\rho}\left(\frac{f^2}{N^2}\,\rho\bar{u}_z\right)_z; \tag{6}$$

where Ω is the angular velocity of the Earth's rotation and N^2 is the buoyant frequency ($N^2 = g$*dlnθ/dz), which represents the static stability.

To offer guidance on the direction of wave propagation within the troposphere and stratosphere (Charney and Drazin, 1961), the index of refraction was calculated in the form given by Matsuno (1970):

$$\mathrm{RI} = \frac{\bar{q}_\emptyset}{a\bar{u}} - \frac{s^2}{a^2\cos^2\emptyset} - \frac{f^2}{4N^2H^2}; \tag{7}$$

where s is the zonal wavenumber and H = 7000 m is the height scale.

According to the downward control principle, the latitudinal and vertical circulation patterns are approximately proportional to the gradients of the vertically integrated wave forces above that level (Haynes et al., 1991). Circulation is thus utilized to distinguish the contributions of GWs and PWs to the residual circulation anomaly. The meridional and vertical residual circulation patterns induced by PW and GW forces are proportional to the vertical and horizontal gradients of the corresponding stream functions (Ψ_{pw}), (Ψ_{gw}) and can be calculated as follows (Haynes et al., 1991):

$$v^*_{(pw,gw)} = -\frac{1}{\rho \cdot cos\varphi} \frac{\partial \Psi_{(pw,gw)}}{\partial z}, \quad (8)$$

$$w^*_{(pw,gw)} = -\frac{1}{a \cdot \rho \cdot cos\varphi} \frac{\partial \Psi_{(pw,gw)}}{\partial \varphi}, \quad (9)$$

where g is the acceleration caused by gravity. Considering that the GW parameters are difficult to present in the MERRA-2 reanalysis dataset, the GW-induced stream function (Ψ_{gw}) can be calculated by the difference between the total (Ψ_{total}) and PW-induced (Ψ_{pw}) stream functions (Karpechko and Manzini, 2012; Lubis et al., 2016), which can be calculated by

$$\Psi_{pw} = \int_z^{\infty} \left\{ \frac{a^{-1} \nabla \cdot \boldsymbol{F}}{(a \cdot cos\varphi)^{-1} \, (\bar{u} \cdot cos\varphi)_{\varphi} - f} \right\} \, \mathrm{d}z', \quad (10)$$

$$\Psi_{total} = \int_z^{\infty} \rho \; cos\varphi \; \cdot v^* \; \mathrm{d}z', \quad (11)$$

The meridional component of the total residual circulation v^* was calculated by equation (4), and $\boldsymbol{F}$ is the Eliassen–Palm flux (Equations 1 and 2). The anomalous temperature, zonal wind, occurrence percentage of the PMCs, and the parameters utilized to diagnose the wave activities are calculated by comparison to the climatological mean from 2004 to 2021. The Cloud Imaging and Particle Size instrument (CIPS), onboard the Aeronomy of Ice in the Mesosphere (AIM) satellite, has been measuring the sunlight scattered by mesospheric clouds at a wavelength of 265 nm since 2007 (Russell et al., 2009; Bailey et al., 2009; Rusch et al., 2009; Benze et al., 2009). The instrument consists of four nadir-viewing cameras covering approximately 2000×1000 km in the polar region, with a horizontal resolution of ~2 km (McClintock et al., 2009). CIPS data were used to obtain the PMC frequency of occurrence.

3 Results

As one of the strongest stratospheric warming events in the SH, the SSW in September 2019 led to dramatic warming (with a maximum of ~ 40 K) in the Antarctic polar stratosphere, associated with significant cooling in the polar mesosphere (with a minimum of ~ -30 K), as suggested by both the MLS observation and MERRS-2 reanalysis dataset (Figures 1a and 1b). Although temperature anomalies are strong, the eastward zonal mean winds significantly weakened from 80 m/s to 20 m/s but did not reverse direction in the September 2019 SSW event (Figure 2b). In the mesosphere, the temperature variation is primarily controlled by adiabatic heating due to upwelling and dowelling. The upper mesospheric temperature decreased significantly between late August and mid-September, corresponding to anomalous upwelling (Figure 2a), which is related to SSW-induced stratospheric perturbations (Figure 2b). During the following months (from mid-September to December), anomalous stratospheric warming and mesospheric cooling propagate downward, resulting in ~15 K warming in the lower stratosphere and ~5 -10 K cooling in the middle and upper stratosphere. The temperature in the upper mesosphere of SH returned to normal during October and became anomalously negative again in November (with a minimum of ~8 K).

Figure 1c presents the climatological mean PMC occurrence percentage observed by the AIM satellite and the 2019 occurrence percentage. The PMC occurrence usually becomes obvious (occurrence percentage > 20%) at the beginning of December (approximately 20 days before the solstice). The Southern Hemisphere PMC occurrence was significantly earlier in 2019, and the probability of occurrence exceeded 20% at the end of November, seven days earlier than the climatological mean.

As the SH polar temperature variation in MERRA2 agrees well with the MLS observations, in the remainder of this study, the possible mechanism by which the 2019 SH SSW could affect the variation in the stratosphere and mesosphere in two months will be investigated based on the MERRA2 reanalysis data.

The PWs, which affect the temperature and wind variation in the stratosphere by providing energy and momentum via their convergence, play an essential role in modulating the vertical coupling from the stratosphere to the mesosphere (Garcia-Herrera et al., 2006; Black & McDaniel, 2007; Li et al., 2013; Yang et al., 2017). In August, the zonal mean eddy heat flux averaged from 45°S to 75°S at 100 hPa (proportional to the vertical component of EP flux) decreased dramatically and persisted until the peak of SSW 2019, indicating that upward PW propagation was strengthened (Figure 2c). The upward propagation of PWs at 100 hPa was weaker than the climatological average after the SSW (from mid-September to mid-October). Meanwhile, the 2019 stratospheric eastward circumpolar flow remained unchanged at

20 m/s, which is different from the weakening of westerly zonal winds in the other years due to seasonal variation (Figure 2b). Anomalous upwelling in the mesosphere becomes much weaker, while anomalous temperature returns to normal by mid-October (Figure 2a). The upward propagation of PWs in the stratosphere was again strengthened from mid-October to November compared to the 2004-2021 mean (Figure 2c). This led to the rapid weakening of the stratospheric zonal wind and a reversal from eastward to westward in the middle of November 2019. The reverse of the stratospheric zonal wind in 2019 occurred approximately half a month earlier than the climatology, indicating an earlier break of the 2019 SH stratospheric polar vortex. Simultaneously, the temperature increase and upwelling were suppressed in the SH polar mesosphere. In summary, the variations in mesospheric temperature, circulation, stratospheric zonal wind, and PW activity are in good agreement with each other two months after SSW 2019 in the SH.

An abnormal upward propagating stratospheric planetary wave, which is suppressed in the first month after SSW but enhanced in the second month after SSW, is closely related to perturbations in the stratosphere and mesosphere from October to November. Nonetheless, as shown in Supporting Information Figure S1, the planetary wave activity in the lower southern troposphere (500 hPa) is stronger than usual during the austral spring of 2019 (September-November) without significant perturbations as in the stratosphere after the SSW event. It is implied that the upward propagation of the PW to the stratosphere is not attributed to variations in the wave source in the lower atmosphere.

Figure 2d shows the anomalous meridional gradient of the potential vorticity ($\bar{q}_{\phi}$) averaged over 50-70°S and 500-200 hPa, which characterizes the tropospheric baroclinic/barotropic instability (when $\bar{q}_{\phi} < 0$) in the SH middle latitudes. The instability ($\bar{q}_{\phi} < 0$) of the background atmosphere could interact strongly with PWs by producing an in situ source of energy for the waves, benefiting the upward propagation and amplification of the PWs (Matsuno, 1970; Hartman, 1983; Meyer & Forbes, 1997).

From August to early September 2019, the tropospheric instability in the SH mid-latitudes was stronger than usual. The atmospheric instability became weaker than usual from mid-September to early October, consistent with the PW variability before and after the SSW event. Since late September, the SH tropospheric instability became enhanced (negative $\bar{q}_{\phi}$ anomalies) compared to the climatology mean and remained stronger than average if a short-lived weakening was neglected in early November. After mid-November 2019, although the tropospheric still has higher instability, the early break of the polar vortex and the reversal of the circumpolar circulation (Figure 2a) prevent the upward propagation of PWs, and the upward-propagating planetary waves in the tropopause region become weaker than usual (Figure 2b).

Due to the wave-mean flow interaction (Baldwin et al., 2003) and “downward control” principle (Haynes et al., 1991; Garcia & Boville, 1994), the significant variations during SSW events tend to progress downward from the upper stratosphere to the lowermost stratosphere in 1-2 months (Baldwin and Dunkerton, 2001; Christiansen, 2005; Sigmond et al., 2013). After the occurrence of SSW in September 2019, the eastward zonal mean zonal winds were suppressed in the midlatitude upper stratosphere (approximately 30-50 km). The negative zonal wind anomalies associated with the warmer-than-normal zonal mean temperature (Figures 1a and 1b) propagated downward. They gradually decreased in October and November, accompanied by increased atmospheric stability in the same region (Figure 3a). Since mid-October 2019, the negative zonal wind anomalies in the stratosphere have descended through the tropopause region and penetrated the lower troposphere, resulting in negative zonal wind anomalies.

The downward propagation of zonal wind anomalies can lead to perturbations in both strong meridional and vertical wind shear, which effectively modulate the variability of atmospheric instability (Figure 3b). According to equation 6, either meridional wind shear or vertical wind shear could contribute to the variability of atmospheric instability. As shown in Figure 3b, the increasing atmospheric instability benefits from perturbation of the vertical and meridional wind shears (term two and term 3 in equation 6) when the anomalous zonal wind penetrates the troposphere around October 15. At the beginning of November 2019, the $\bar{q}_{\phi}$ anomalies become positive, primarily due to the vertical zonal wind shear variation. This suppressed instability corresponds well to the 100 hPa eddy heat flux variations (Figure 2b).

In the SH spring of 2019, the enhanced activity of PWs persists in the lower troposphere in the latitude range of 30-70°S (Figure S1, Figure 3c and Figure 3d). However, during the first month following the SSW (September 17 to October 15), anomalous Eliassen-Palm (EP) flux from the lower troposphere tends to propagate equatorward to the area with higher atmospheric instability (with negative $\bar{q}_{\emptyset}$) rather than traveling upward into the stratosphere across the midlatitude upper stratosphere (Figure 3c). At the lower latitudes (40°S and equatorward), the atmospheric instability increases in the upper troposphere, which is related to the positive phase of the tropospheric SAM in the SH mentioned by Jucker et al. (2022). The anomalous $\bar{q}_{\emptyset}$ in the upper troposphere increased near 60°S, indicating higher barotropic/baroclinic stability of the atmosphere and inhibiting the upward and poleward propagation of the PWs. Due to the suppressed upward propagation of PWs into the stratosphere, westward momentum transport into the SH stratosphere decreased, and the anomalous westward zonal wind became less evident.

As discussed above, from October 15 to November 15, as the negative zonal wind anomalies penetrate the troposphere, the atmospheric instability increases in the midlatitude troposphere, benefiting the amplification of the PWs. Thus, the enhanced EP flux is transported from the lower troposphere toward midlatitude and vertically into the troposphere (green vector in Figure 3d).

To diagnose the effect of atmospheric variation on PW propagation and refraction, the index of refraction (RI), which is a good indicator of the PW propagation direction in the stratosphere, is also investigated. PWs are preferentially ducted toward regions with a more positive index of refraction and refracted away from regions with a more negative RI (Andrews et al. 1987). The variation in RI is affected by barotropic/baroclinic instability, zonal wind (2nd term in equation 7), and static stability (3rd term in equation 7).

Since the occurrence of SSW, the refractive index in the stratosphere has decreased at mid-latitudes and increased at high latitudes due to variations in barotropic/baroclinic instability caused by anomalies in wind shear, zonal wind, and static stability (Jucker et al., 2022). From October 15 to November 15, the enhanced PWs propagating upward into the stratosphere from mid-latitudes tend to deflect poleward and modulate the circumpolar flow in the high latitudes. This accelerates the seasonal reversal of the eastward wind to the westward wind in SH and leads to the complete break of the SSPV in mid-November (Figure S2).

The climatological zonal mean zonal wind at the SH high latitudes in November is characterized by a weak eastward wind in the lower stratosphere and an increased westward wind in the upper stratosphere and lower mesosphere. Due to the early break of the SH polar vortex in November 2019, the filtering of eastward and upward-propagating GWs by eastward zonal wind is replaced by the filtering of the westward GWs by the westward zonal wind in the lower stratosphere. In the upper stratosphere, more westward-propagating GWs are filtered by the strengthened westward zonal wind. As a result of the net effect of zonal wind filtering, the eastward GW forcing is thus enhanced in the SH mesosphere, strengthening the SH mesospheric residual meridional circulation with anomalous SH polar mesosphere upwelling (Figure 4a). This suggests that the SH polar mesopause temperature is controlled by the stratospheric zonal wind in the SH high latitudes via the gravity wave filtering process (Karlsson et al., 2011; Li et al., 2016; Yang et al., 2017).

According to the downward control principle, the meridional circulation patterns are approximately proportional to the gradients of the vertically integrated wave force above that level (Haynes, 1991). Thus, the contributions of GWs and PWs to the residual circulation anomaly could be distinguished by the vertical and horizontal gradients of the corresponding stream functions, as shown in equations 8-11. Due to the early break of the stratospheric polar vortex, the upwelling of the meridional circulation was enhanced in the SH mesopause primarily due to the eastward GWs in the second half of November (see Figure 4b). The enhanced upwelling in the SH polar region led to as low as -10 K temperature anomalies from 60 to 80 km, 60°-90°S (~ -10 K) through adiabatic cooling. It increased the water vapor mixing ratio from 70 to 80 km (with an increase of ~0.2 ppmv, as high as 10% of background H2O) through dynamic transport. The early onset of PMCs in the SH mesosphere in November 2019 thus benefited from both the temperature and water vapor variation in the upper mesosphere.

4. Summary and Discussion

The emerging picture of the mechanisms can be summarized as follows: as the

SSW event occurred in September 2019, the stratospheric polar vortex significantly weakened with the much weaker circumpolar eastward zonal wind, while the zonal wind in the troposphere, however, was mainly eastward. The barotropic/baroclinic instability, primarily controlled by the vertical and meridional wind shear, is weaker (positive anomalous meridional gradient of the potential vorticity) in the mid-latitudes of the upper troposphere for the first month after the SSW (September 17 to October 15, 2019). The decreased barotropic/baroclinic instability indicates less energy for amplifying the waves passing by, causing perturbations from the troposphere to deflect equatorward close to the tropopause rather than continuing vertically into the stratosphere. Crucially, the deflection of EP fluxes leads to less westward momentum transport into the SH stratosphere, preventing the seasonal weakening of the polar vortex.

Under the influence of the downward control and wave-mean interaction, the westward anomalies of the zonal wind propagate downward and reach the troposphere after October 15, 2019. The anomalous zonal wind thus modulates the vertical and meridional wind shear. It increases the atmospheric barotropic/baroclinic instability in the midlatitude troposphere, which provides energy to amplify the PWs passing through and removes the midlatitude propagation barrier for EP fluxes. As a result, more EP flux PWs from the lower troposphere can propagate into the stratosphere (Figure 3d). The refractive index influenced by barotropic/baroclinic instability and static stability anomalies (Jucker et al., 2022) guides the PWs to propagate poleward in the stratosphere. The westward momentum transport by the anomalous PWs decreases the circumpolar eastward wind and benefits the early break of the stratospheric polar vortex.

The early reversal of the SH stratospheric zonal wind in November 2019 caused the filtering of westward GWs by westward zonal wind rather than filtering the eastward GWs by the eastward zonal wind in the lower stratosphere. More westward-propagating GWs enhance the mesospheric meridional mean residual circulation, including anomalous upwelling over the polar region and northward flow in the upper mesosphere. The enhanced upwelling in the SH polar region is key to cooling the polar mesosphere and increasing the water vapor mixing ratio. Both contributed to the early onset of PMCs in the SH mesosphere in November 2019.

To conclude, our results indicate a mechanism in which the early spring stratospheric perturbation could affect the vertical coupling from the troposphere to the mesosphere in early winter. While we studied this mechanism concerning the 2019 SH September SSW, the early break of the SSPV, and the response in the polar SH mesosphere in November 2019, it does not have to be limited to such events. It can be expected to be relevant whenever lower stratospheric and upper tropospheric barotropic/baroclinic instability interacts with the zonal wind anomalies and PW activities. Thus, future work will explore the dynamical coupling during other occurrences of stratospheric perturbation in both the Southern and Northern Hemispheres. In addition to the dynamics process, the interplay between dynamics and radiation heating could influence the long-lasting coupling process induced by the stratospheric perturbation, but further work is required to explore this.

Acknowledgment

This work was supported by the National Natural Science Foundation of China grants (42130203, 41874180, 41974175, 41831071); the B-type Strategic Priority Program of the Chinese Academy of Sciences, grant no. XDB41000000; the pre-research project on Civil Aerospace Technologies no. D020105 funded by China’s National Space Administration; and the Open Research Project of Large Research Infrastructures of CAS –“Study on the interaction between low/mid-latitude atmosphere and ionosphere based on the Chinese Meridian Project.” XW is supported by the NSF via the NCAR's Advanced Study Program Postdoctoral Fellowship.

Data Availability Statement

The Cloud Imaging and Particle Size (CIPS) observed by AIM/aura are available at https://lasp.colorado.edu/aim/. The subsets of MERRA-2 tavg3_3d_asm_Nv: 3d,3-Hourly, Time-Averaged, Model-Level, Assimilation, Assimilated Meteorological Fields V5.12.4 data are downloaded at https://disc.gsfc.nasa.gov/datasets/M2T3NVASM_5.12.4/summary?keywords=MERRA-2%20tavg3_3d_asm.

The Aura/MLS temperature and water vapor mixing ratio measurements are downloaded at https://acdisc.gesdisc.eosdis.nasa.gov/data/Aura_MLS_Level2/ML2T.005/ and https://acdisc.gesdisc.eosdis.nasa.gov/data/Aura_MLS_Level2/ML2H2O.005/, respectively.

Figure cations

Figure 1. Anomalous SH polar cap (65°-90°S) temperature from August 2019 to December 2019 from (a) MLS observations and (b) MERRA2 reanalysis datasets; (c) the mean SH PMC occurrence percentage derived from AIM/aura from 2007 to 2021 (thick black line) for the solstice. The blue line indicates the SH PMC occurrence during 2019, and the gray shading indicates 1 standard deviation.

Figure 2. (a) MERRA2 zonal mean temperature anomalies from 70-80 km, averaged over 65°S and poleward (red line and shading), and the vertical component of the residual circulation anomalies in the SH polar mesosphere (80°S and poleward, 65-80 km, green line, and shading) from August to December. (b) MERRA2 zonal mean zonal wind at 60°S, 10 hPa from August to December (light gray lines). (c) Anomalous eddy heat flux averaged over 45-75°S, 100 hPa from August 2019 to December 2019. (d) The meridional gradient of potential vorticity averaged over 50-70°S from August 2019 to December 2019. The purple line denotes 2019, the thick black line indicates the mean from 2004 to 2018, and the red and blue shadings indicate positive and negative

anomalies compared to the climatological mean.

Figure 3. (a) Zonal mean zonal wind anomalies (shading) superimposed by the anomalous meridional gradient of the potential vorticity ($\bar{q}_{\emptyset}$) multiplied by a (the Earth's radius) at 60°S, 5-50 km (contours, white solid lines indicate positive anomalies, white dashed lines indicate negative anomalies, and the contour interval is 30 m^{-1}) f for August-December 2019. The vertical red dashed line indicates the occurrence of the SSW, while the vertical gray dashed line indicates the date of Oct 15. The horizontal red solid line denotes the location of the lowermost stratosphere. (b) The anomalous $\bar{q}_{\emptyset} * a$ due to the meridional wind shear (upper) and vertical wind shear at 60°S from 5 to 15 km for August-December 2019; (c) The latitude-altitude cross-section for the SH $\bar{q}_{\emptyset}$ anomalies (shading), EP flux (green vector) and the wavenumber 1 refractive index multiplied by a^2 (contour lines, the solid and dashed gray lines indicate 10 and -10, respectively) averaged from September 17 to October 15, 2019; (d) is the same as (c) but for the period from October 15 to November 15, 2019.

Figure 4. (a) Latitude versus altitude cross section of the anomalous meridional residual mean circulation (m/s, streamlines), zonal mean temperature (K, shading) and zonal mean volume mixing ratio of water vapor (ppmv, contours) from November 15 to 30, 2019; (b) anomalous vertical residual circulation (cm s-1) averaged over 85°S-70°S from 20 to 80 km from November 15 to 30, 2019, the thick black line associated with the gray shading indicate the total vertical residual circulation anomalies, while the red and blue lines associated with the red and blue shadings indicate the vertical residual

circulation anomalies due to none-resolved and resolved waves, respectively.

References

Andrews, D. G., Holton, J. R., & Leovy, C. B. (1987). Middle atmosphere dynamics. San Diego, CA: Academic Press.

Bailey, S. M., G. E. Thomas, D. W. Rusch, A. W. Merkel, C. D. Jeppesen, J. N. Carstens, C. E. Randall, W. E. McClintock, and J. M. Russell III (2009), Phase functions of polar mesospheric cloud ice as observed by the CIPS instrument on the AIM satellite. *Journal of Atmospheric and Solar-Terrestrial Physics*, 71, 373–380, https://doi.org/10.1016/j.jastp.2008.09.039.

Baldwin, M. P., & Dunkerton, T. J. (2001). Stratospheric harbingers of anomalous weather regimes. *Science*, 294(5542), 581–584. https://doi.org/10.1126/science.1063315.

Baldwin MP, Stephenson DB, Thompson DWJ, Dunkerton TJ, Charlton AJ, O'Neill A. (2003). Stratospheric memory and extended-range weather forecasts. *Science*, 301: 636–640. https://doi.org/10.1126/science.108714

Baldwin M, Hirooka T, O'Neill A, Shigeo Yoden. (2003). Major stratospheric warming in the Southern Hemisphere in 2002: dynamical aspects of the ozone hole split. *SPARC Newsletter*, 20, 24–26.

Baldwin, M. P., Ayarzagüena, B., Birner, T., Butchart, N., Butler, A. H., Charlton-

Perez, A. J., et al. (2021). Sudden stratospheric warmings. *Reviews of Geophysics*, 59, e2020RG000708. https://doi.org/10.1029/2020RG000708

Benze, S., C. E. Randall, M. T. DeLand, G. E. Thomas, D. W. Rusch, S. M. Bailey, J. M. Russell III, W. McClintock, A. W. Merkel, and D. Jeppesen (2009), Comparison of polar mesospheric cloud measurements from the cloud imaging and particle size experiment and the solar backscatter ultraviolet instrument in 2007, *Journal of Atmospheric and Solar-Terrestrial Physics*, 71, 365–372, https://doi.org/10.1016/j.jastp.2008.07.014.

Black, R. X., and B. A. McDaniel (2007), Interannual variability in the Southern Hemisphere circulation organized by stratospheric final warming events. *Journal of Atmospheric Science*, 64, 2968–2974, https://doi.org/10.1175/JAS3979.1.

Butler, A. H., Seidel, D. J., Hardiman, S. C., Butchart, N., Birner, T., & Match, A. (2015). Defining sudden stratospheric warmings. *Bulletin of the American Meteorological Society*, 96(11), 1913–1928. https://doi.org/10.1175/Bams-D-13-00173.1.

Charney, J. G., and P. G. Drazin. (1961). Propagation of planetaryscale disturbances from the lower into the upper atmosphere. *Journal of Geophysical Research*, 66, 83–109, https://doi.org/10.1029/JZ066i001p00083.

Christiansen B. (2005). Downward propagation and statistical forecast of the near-surface weather. *Journal of Geophysical Research*, 110: D14104. https://doi.org/10.1029/2004JD005431.

Garcia, R. R., & Boville, B. A. (1994). Downward control of the mean meridional circulation and temperature distribution of the polar winter stratosphere. *Journal of the Atmospheric Sciences*, 51, 2238–2245.

Gelaro, R., McCarty, W., Suarez, M. J., Todling, R., Molod, A., Takacs, L., et al. (2017). The Modern-Era retrospective analysis for Research and Applications, version 2 (MERRA-2). *Journal of Climate*, 30(13), 5419–5454. https://doi.org/10.1175/JCLI-D-16-0758.1.

Haynes, P. H., McIntyre, M. E., Shepherd, T. G., Marks, C. J., and Shine, K. P. (1991). On the “downward control” of extratropical diabatic circulations by eddy induced mean zonal forces. *Journal of Atmospheric Science,* 48(4), 651–678. https://doi.org/10.1175/1520-0469(1991)048<0651:Otcoed>2.0.Co;2

Hartman, D. L. (1983). Barotropic instability of the polar night jet stream. *Journal of Atmospheric Science*, 40, 817-835.

Hervig, M. E., Siskind, D. E., Bailey, S. M., & Russell, J. M., III (2015). The influence of PMCs on water vapor and drivers behind PMC variability from SOFIE observations. *Journal of Atmospheric and Solar-Terrestrial Physics*, 132, 124–134. https://doi.org/10.1016/j.jastp.2015.07.010.

Hervig, M. E., M. H. Stevens, L. L. Gordley, L. E. Deaver, J. M. Russell III, and S. M. Bailey (2009), Relationships between polar mesospheric clouds, temperature, and water vapor from Solar Occultation for Ice Experiment (SOFIE) observations. *Journal of Geophysical Research*, 114, D20203, https://doi.org/10.1029/2009JD012302.

Jucker, M., & Goyal, R. (2022). Ozone-forced Southern Annular Mode during Antarctic stratospheric warming events. *Geophysical Research Letters*, 49, e2021GL095270. https://doi.org/10.1029/2021GL095270.

Karpechko, A. Y., and Manzini, E. (2012). Stratospheric influence on tropospheric climate change in the Northern Hemisphere. *Journal of Geophysical Research-Atmospheres*, 117(D5), D05133. https://doi.org/10.1029/2011JD017036.

Li, T., N. Calvo, J. Yue, X. Dou, J. M. Russell, M. G. Mlynczak, C.-Y. She, and X. Xue. (2013). Influence of El Niño–Southern Oscillation in the mesosphere. *Geophysical Research Letters*, 3292–3296. https://doi.org/10.1002/grl.50598.

Li, T., Calvo, N., Yue, J., Russell, J. III, Smith, A., Mlynczak, M., et al. (2016). Southern hemisphere summer mesopause responses to El Niño-Southern Oscillation. *Journal of Climate*, 29(17), 6319–6328. https://doi.org/10.1175/JCLI-D-15-0816.1

Lindzen, R. S. (1981), Turbulence and stress owing to gravity wave and tidal breakdown. *Journal of Geophysical Research*, 86, 9707–9714. https://doi.org/10.1029/JC086iC10p09707.

Livesey, N., Read, W., Wagner, P., Froidevaux, L., Lambert, A., Manney, G., et al. (2017). Version 4.2 x Level 2 data quality and description document. *JPL D-33509 Rev*. B.C.

Lubis, S. W., Omrani, N. E., Matthes, K., and Wahl, S. (2016). Impact of the antarctic ozone hole on the vertical coupling of the stratosphere mesosphere-lower thermosphere system. *Journal of Atmospheric Science*, 73(6), 2509–2528. https://doi.org/10.1175/Jas-D-15-0189.1

Matsuno, T. (1970). Vertical propagation of stationary planetary waves in the winter Northern Hemisphere. *Journal of Atmospheric Science*, 27, 871–883, https://doi.org/10.1175/1520-0469(1970)027,0871:VPOSPW.2.0.CO;2.s

McClintock, W. E., D. W. Rusch, G. E. Thomas, A. W. Merkel, M. R. Lankton, V. A. Drake, S. M. Bailey, and J. M. Russell III (2009), The cloud imaging and particle size experiment on the Aeronomy of Ice in the Mesosphere mission: Instrument concept, design, calibration, and on-orbit performance. *Journal of Atmospheric and Solar-Terrestrial Physics*, 71, 340–355, https://doi.org/10.1016/j.jastp.2008.10.011.

McLandress, C. (1998), On the importance of gravity waves in the middle atmosphere and their parameterization in general circulation models. *Journal of Atmospheric and Solar-Terrestrial Physics*, 60, 1357–1383. https://doi.org/10.1016/S1364-6826(98) 00061-3.

Meyer, C. K., & Forbes, J. M. (1997). A 6.5-day westward propagating planetary wave: Origin and characteristics. *Journal of Geophysical Research: Atmospheres*, 102(D22), 26173–26178. https://doi.org/10.1029/97jd01464.

Plumb, R. A., and K. Semeniuk. (2003). Downward migration of extratropical zonal wind anomalies, *Journal of Geophysical Research*, 108(D7), 4223.

https://doi.org/10.1029/2002JD002773.

Schwartz, M. J., and Coauthors, 2008: Validation of the Aura Microwave Limb Sounder temperature and geopotential height measurements. *Journal of Geophysical Research*, 113, D15S11, https://doi.org/10.1029/2007JD008783.

Rusch, D. W., G. E. Thomas, W. McClintock, A. W. Merkel, S. M. Bailey, J. M. Russell III, C. E. Randall, C. D. Jeppesen, and M. Callan (2009), The cloud imaging and particle size experiment on the Aeronomy of Ice in the Mesosphere mission: Cloud morphology for the northern 2007 season, *Journal of Atmospheric and Solar-Terrestrial Physics*, 71, 356–364, https://doi.org/10.1016/j.jastp.2008.11.005.

Russell, J. M., III, et al. (2009), The Aeronomy of Ice in the Mesosphere (AIM) mission: Overview and early science results, *Journal of Atmospheric and Solar-Terrestrial Physics*, 71, 289–299, https://doi.org/10.1016/j.jastp.2008.08.011.

Shen, X., Wang, L., & Osprey, S. (2020a). The Southern Hemisphere sudden stratospheric warming of September 2019. *Science Bulletin*, 65(21), 1800–1802. https://doi.org/10.1016/j.scib.2020.06.028

Shen, X., Wang, L., & Osprey, S. (2020b). Tropospheric forcing of the 2019 Antarctic sudden stratospheric warming. *Geophysical Research Letters*, 47, e2020GL089343. https://doi.org/10.1029/2020GL089343.

Shepherd, T. G. (2000), The middle atmosphere. *Journal of Atmospheric and Solar-Terrestrial Physics*, 62, 1587–1601, https://doi.org/10.1016/S1364-

6826(00)00114-0.

Sigmond M, Scinocca JF, Kharin VV, Shepherd TG. (2013). Enhanced seasonal forecast skill following stratospheric sudden warmings. *Nature Geoscience*. 6: 98–102. https://doi.org/10.1038/ngeo1698.

Karlsson, B., C. E. Randall, T. G. Shepherd, V. L. Harvey, J. Lumpe, K. Nielsen, S. M. Bailey, M. Hervig, and J. M. Russell III. (2011). On the seasonal onset of polar mesospheric clouds and the breakdown of the stratospheric polar vortex in the Southern Hemisphere. *Journal of Geophysical Research*, 116, D18107, https://doi.org/10.1029/2011JD015989.

Chandran, A., & Collins, R. L. (2014). Stratospheric sudden warming effects on winds and temperature in the middle atmosphere at middle and low latitudes: A study using WACCM. *Annales Geophysics*, 32(7), 859–874. https://doi.org/10.5194/angeo-32-859-2014.

Thompson, D. W. J., and S. Solomon (2002), Interpretation of recent Southern Hemisphere climate change, *Science*, 296, 895–899.

Thompson, D. W. J., M. P. Baldwin, and S. Solomon (2005), Stratosphere-troposphere coupling in the Southern Hemisphere. *Journal of Atmospheric Science*, 62, 708–715.

Waters, J. W., Froidevaux, L., Harwood, R. S., Jarnot, R. F., Pickett, H. M., Read, W. G., et al. (2006). The Earth observing system microwave limb sounder (EOS MLS) on the aura satellite. *IEEE Transactions on Geoscience and Remote*

Sensing, 44(5), 1075–1092. https://doi.org/10.1109/Tgrs.2006.873771.

Yamazaki, Y., Matthias, V., Miyoshi, Y., Stolle, C., Siddiqui, T., Kervalishvili, G., et al. (2020). September 2019 Antarctic sudden stratospheric warming: Quasi-6-day wave burst and ionospheric effects. *Geophysical Research Letters*, 47, e2019GL086577. https://doi.org/10.1029/2019GL086577.

Yang, C., Li, T., Smith, A. K., & Dou, X. (2017). Response of the Southern Hemisphere middle atmosphere to the Madden-Julian Oscillation during austral winter using the Specified-Dynamics Whole Atmosphere Community Climate Model. *Journal of Climate*, 30(20), 8317–8333. https://doi.org/10.1175/JCLI-D-17-0063.1

Supporting Information for " The delayed response of the troposphere-stratosphere-mesosphere coupling to the 2019 southern SSW"

Chengyun Yang[1,2,3], Tao Li[1,2,3*], Dexin Lai[1,2,3], Xinyue Wang[5], Xianghui Xue[1,2,3] and Xiankang Dou[1,2,3,4]

[1]CAS Key Laboratory of Geospace Environment, School of Earth and Space Sciences, University of Science and Technology of China, Hefei, Anhui, China

[2]Mengcheng National Geophysical Observatory, School of Earth and Space Sciences, University of Science and Technology of China, Hefei, China

[3]CAS Center for Excellence in Comparative Planetology, University of Science and Technology of China, Hefei, Anhui, China

[4]School of Electronic Information, Wuhan University, Wuhan, Hubei, China

[5]Atmospheric Chemistry Observation and Modeling, National Center for Atmospheric Research, Boulder, CO, USA

Corresponding author: Tao Li (litao@ustc.edu.cn)

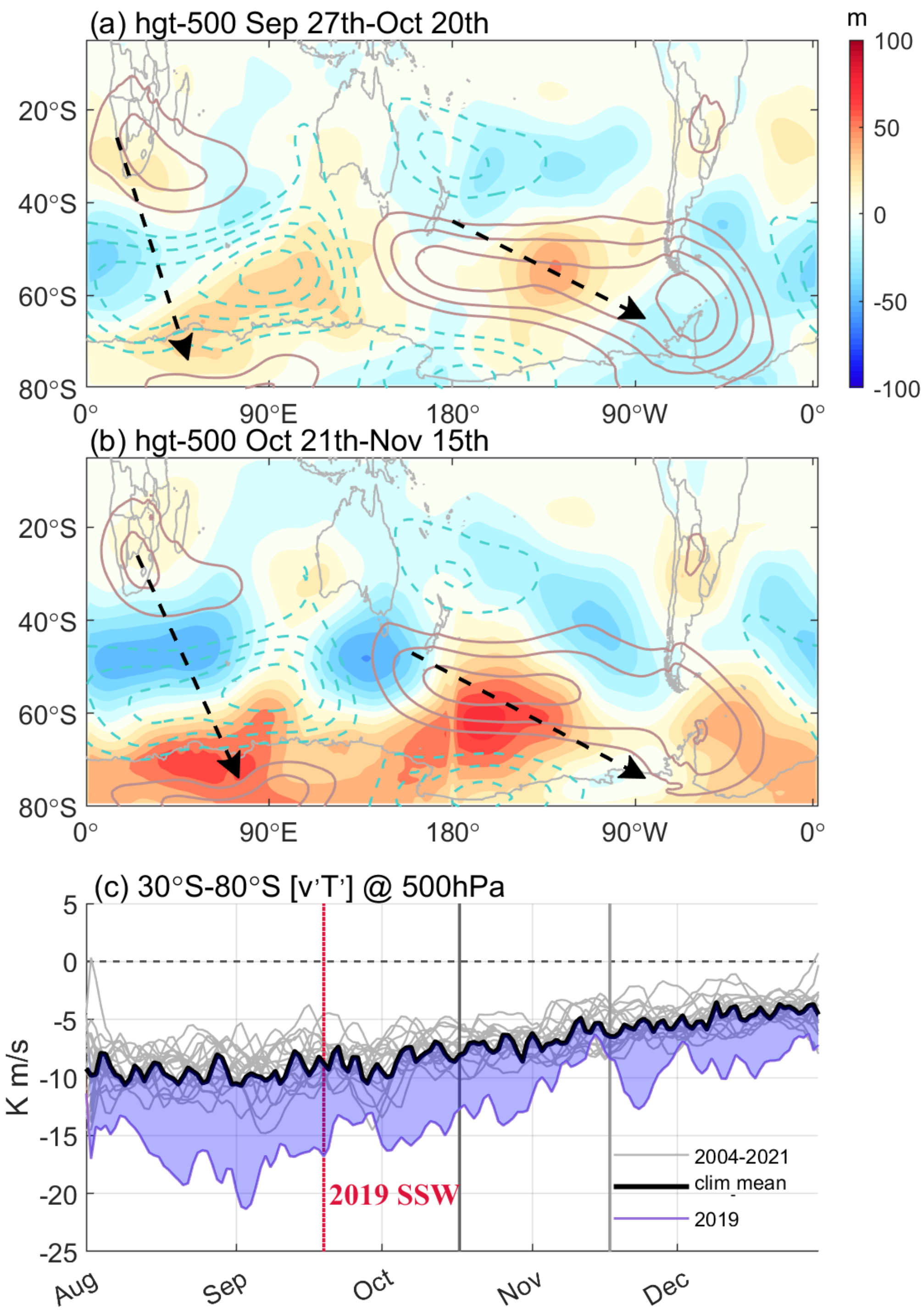

Figure S1. MERRA2 500 hPa anomalous geopotential height from (a) September 27th to October 21st and (b) September 27th to October 21st. The shadings indicate the anomalies during 2019, while the contours indicate the climatological distribution of the zonal anomalous geopotential height at 500 hPa. (c) Anomalous eddy heat flux averaged over 30-80°S, 500 hPa from August 2019 to December 2019. The purple line denotes the year 2019, the black thick line indicates the mean from 2004 to 2018, and the red and blue shadings indicate positive and negative anomalies compared to the climatological mean.

Description:

To examine the variations of the tropospheric planetary wave source from October to November, the potential height anomalies at 500 hPa during two periods (from 27th September to 20th October and from 21st October to 20 October, respectively) after 2019 SSW, associated with the climatological mean for these periods are shown in Figure R1. During the two periods following the 2019 SSW event (corresponding to enhanced and suppressed upward propagating PWs in the stratosphere at mid-latitude and high latitudes, respectively, as shown in Figure 2 in the revised manuscript), the distributions of the tropospheric geopotential height anomalies are similar to each other, characterized by two PW train.

One is that the anomalous planetary wave train extending from southern Africa to Antarctica, consisting of positive anomalies to the south of Africa, negative anomalies extending from the south Atlantic to the south Indian Ocean between Africa and Antarctic, the positive anomalies over the Antarctic, coincides with the distribution of climatical zonal anomalous geopotential heights, leading to the increased planetary wave activity in the SH troposphere. The anomalous wave trains over the southern Pacific are different between the two periods. From September 27th to October 15th, the anomalous wave train consisted of negative anomalies to the east of New Zealand, positive anomalies over Southern Pacific centered at approximately 60°S, 130°W, and negative anomalies centered at the Antarctic Peninsula. From October 16th to November 15th, the anomalous wave train extends from the negative anomalies to the south of Australia to the positive anomalies over the central Southern Pacific. Although the wave train from the Southern Pacific is more intense in the latter period than in the former, the positive and negative anomalies together overlapping the climatological mean zonal positive anomalies that span the mid and high latitudes of the South Pacific implies little contribution to the variation of the total planetary wave activity.

As a result, 500 hPa geopotential height anomalies generally lead to an enhanced planetary wave activity in the SH troposphere during October and November 2019, as also suggested by the anomalous eddy heat flux shown in Fig. R1c. Continuously stronger tropospheric planetary wave activity than usual is inconsistent with stratospheric PWs, which were first suppressed and then strengthened (Figure 2 in the revised manuscript). We, therefore, think that the change in the upward PW propagation process is the main reason for the variation in stratospheric PWs after SSW rather than the change of the tropospheric plane-wave source.

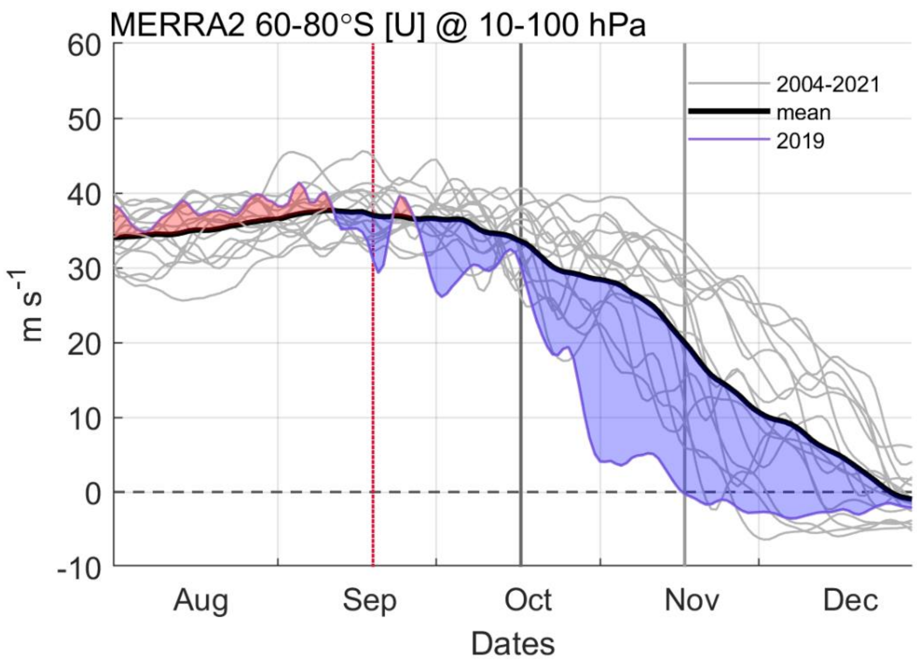

Figure S2. MERRA2 zonal mean zonal wind averaged at 60°-80°S, 10 hPa from August to December (light gray lines), the purple line denotes the zonal wind of 2019, the black thick line indicates the mean zonal wind from 2004 to 2018, the red and blue shadings indicate positive and negative anomalies compare to the climatological mean.